Hindawi
Shock and Vibration
Volume 2022, Article ID 8620943, 10 pages
https://doi.org/10.1155/2022/8620943

Research Article

A Film Bulk Acoustic Resonator-Based Sensor with AlN Piezoelectric Material for Detecting Ethanol and Acetone

Jieyi Zhu,[1] **Meiyan Feng**,[2] **and Guofu Lian**[2]

[1]*School of Electronic, Electrical Engineering and Physics, Fujian University of Technology, Fuzhou 350108, China*
[2]*School of Mechanical and Automotive Engineering, Fujian University of Technology, Fuzhou 350108, China*

Correspondence should be addressed to Jieyi Zhu; zhujieyi@mail.ustc.edu.cn

Received 18 July 2022; Revised 17 September 2022; Accepted 21 October 2022; Published 21 November 2022

Academic Editor: Sami El-Borgi

Measurement of a volatile solution is essential for laboratory safety and hospital clinic safety. In this paper, we present an ethanol-sensing and acetone-sensing device using an AlN piezoelectric material-based film bulk acoustic resonator (FBAR). In order to realize volatile solution sensing, the AlN-based FBAR was designed, fabricated, and characterized. In our sensor structure, the upper electrode is a Ti/Au (30 nm/150 nm) composite electrode, the bottom electrode is Mo material with 150 nm thickness, and the piezoelectric sensing material is 0.8 μm thickness AlN. We conducted the experiment of ethanol measurement and acetone measurement by using this FBAR detector on the probe station within the vector network analyzer. The resonance frequency of the FBAR detector decreased as the concentration of ethanol increases, while under the circumstance of acetone concentration increasing, the detector's response is the opposite. The sensing mechanisms of both ethanol measurement and acetone measurement are discussed in this paper, demonstrating that this FBAR detector could be able to distinguish acetone from ethanol due to different sensing mechanisms.

1. Introduction

During the last decade, the study of film bulk acoustic resonators (FBAR) has been used for the design of biochemical sensors. Compared to traditional detection method, including solution chromatography (GC) and liquid chromatography (LC) [1], FBAR detectors bring low fabrication cost and short detection time, together with the advantage of being compact and easy to carry [2]. Our study group in university focus on the design, fabrication, and measurement of micro biochemical sensors, thus, FBAR chips for the use of volatile solution sensing have come into our vision. For sensing principle, the detector mechanism of FBAR is similar as quartz crystal microbalance (QCM), all belonging to mass-sensitive detectors [3]. Under normal circumstance, the mass-sensitive detector is proportional to the fundamental resonance frequency. Once the biomedical target molecule binds to the piezoelectric area of the FBAR sensor, the increasing mass would lead to a natural resonance frequency decrease [4]. The film bulk acoustic resonator (FBAR) usually consists of a sputtered piezoelectric thin film (ZnO/AlN) sandwiched by two metal layers (top and bottom electrodes). The top and bottom electrode materials could be Au, Al, Mo, or composite electrodes such as Ti/Au, Ni/Au. Under the certain frequency, a resonance condition occurs of the thickness of the piezoelectric material thin film d is equal to an integer multiple of a half of the acoustic wavelength λ. Before the appearance of FBAR detectors, there have been other kinds of traditional filters like surface acoustic wave (SAW) and bulk acoustic surface (BAW). Different with the former traditional filters, the FBAR sensors are fabricated on silicon substrate by using MEMS technology and piezoelectric membrane [5]. Thus, the production of FBAR sensors would overcome the shortage of the former traditional filters, becoming vital cells in the next generation of wireless communication products. The FBAR would satisfy multifunction, multiband, and multiprotocol systems, which is the development direction of filters in the new century. For piezoelectric material choice, we usually have three selections: AlN, ZnO, and PZT [6]. Comparatively, ZnO FBAR would allow sensing characteristic to many

targets, while our sputtering equipment is more inclined to prepare AlN piezoelectric membrane. Although PZT brings higher piezoelectric properties, its fabrication process is much more difficult than AlN. And the cost of PZT is more expensive than that of AlN. Here, in this paper we report an AlN-based film bulk acoustic resonator (FBAR) detector for sensing ethanol and acetone, the bottom electrode is a 150 nm Mo electrodes, the top electrode is a Ti/Au composite electrode with a corresponding thickness of 30 nm/150 nm.

With the increasing importance of clinical diagnosis and medical technology, studies of biochemical sensors have been research hotspots in recent years [7]. Among numerous micro chemical sensors, FBAR has been used for important liquid and gas-phase chemical substance detection due to its significant performance and sensitivity [8]. For instance, Zhang et al. 's paper introduced the design of an FBAR gas sensor based on ZnO film [9]. A. Kumar and Prajesh's review also introduced the potential of FBAR for gas sensing applications [10]. For liquid detection, A. Soltan et al. 's paper presented the FBAR microwave sensor for liquid classification [11]. Lin et al. 's study has revealed an FBAR based explosive trace detection sensor for TNT detection [12]. FBAR sensor could also be utilized to predict frequency shift in viscous media due to Zhao et al. 's study [13]. Furthermore, FBAR sensors could be modified and functionalized to be pesticide detectors for organophosphate measurement [14]. In our work, we finished the FBAR chip and produced this sensor to distinguish two common laboratory volatile gases. Ethanol and acetone are commonly used volatile chemicals in laboratory and medical occasion. Semiconductor sensors are widely used and accepted as ethanol and acetone detectors. There are many advantages for these kinds of semiconductor sensors, including low fabrication cost, sensitivity and sufficient detection limit. However, there is still one need to distinguish acetone vapor from ethanol vapors effectively. In our study, we fabricated the AlN-based FBAR sensor and conducted the experiment to measure ethanol and acetone, we have observed different responses. Then, the sensing mechanism of the FBAR sensor for these two volatile solutions is described and explained.

2. Sensor Structure

In our design, the sensor structure is one AlN-based FBAR sensor. The sputtered piezoelectric thin film of 0.8 μm AlN is sandwiched by two metal electrodes. The top electrode of this FBAR is Ni/Au with the thickness of 30 nm/150 nm; the bottom electrode is 150 nm Mo. We choose the p-doped Si substrate; one side of the substrate is deposited by the AlN/Mo/AlN structure. The sputtering process of the 150 nm Mo film was conducted by the SPTS physical vapor deposition (PVD) system, the deposition is controlled by the argon flow. While the sputtering process of AlN piezoelectric material was also conducted by the SPTS physical vapor deposition (PVD) system, which allow the nitrogen solution and argon solution to flow to the Al target inside the equipment. The top electrode material, Ti/Au was conducted by the electron beam evaporation equipment, ULVAC Ei-5z.

Before the experiment, we need to fix the FBAR sensor on to the platform of the probe station by magnetic adsorption, under probe station' microscope view, the FBAR arrays' surface are shown in Figure 1. During the observation process, silica gel was coated around the detection area to form a chamber. The AlN piezoelectric material was inside the chamber. For each one-detection experiment, we dropped 10 μL solutions to be detected on to the AlN piezoelectric area inside the chamber. After about 10 s we recorded the resonance frequency of the chosen experimental module of the FBAR arrays. The resonance frequency of the FBAR was monitored with an Agilent E5071C network analyzer (Agilent, Santa Clara, CA). The probe station and Keithley source meter were also prepared to help record the experimental data. For sensing mechanism, the FBAR detection method is based on the inverse piezoelectric effect, when electrical signal is applied to the FBAR sensor, the electrical signal could be transformed the electrical signal into sound signal. The resonance frequency of this sound signal would represent the information of piezoelectric thin films and analysts. From the resonance frequency data, we could indirectly obtain the information of analyst to be detected.

In summary, in this paper, FBAR sensors are designed for sensing volatile solutions such as acetone and ethanol, by using the AlN piezoelectric material. FBAR technology could also be utilized to produce oscillators, duplexers, and other high-performance frequency devices. Compared to graphene sensors, the piezoelectric material AlN could be deposited by specific magnetic sputtering equipment within fewer fabrication hours, which is more efficient than the graphene fabrication period, avoiding graphene transfer craft by human labour. The sensor structure is shown in Figure 2.

3. Fabrication and Characterization

3.1. Fabrication of Microchip. In the beginning of sensor design, we finished our FBAR layout design using the software L-Edit. Along with the designed FBAR layout, we set the fabrication steps as the following procedure. The first step is the growth of AlN/Mo/AlN material on the silicon substrate by magnetron sputtering. The growth parameters of AlN and Mo during sputtering process are listed in Table 1. An AlN thin film was deposited in the magnetron sputtering process, which utilized nitrogen flow and argon flow to the Al target. The growth parameters of AlN and Mo are listed in Table 1. Second, the bottom electrode deposition was done. The photolithography process was conducted on the front side of the chip, and then, the step electron beam evaporation for 150 nm Mo was finished. Then we conducted the stripping by the ultrasound metal stripping method. For the third step, the sputtering and patterning of the piezoelectric thin films were accomplished. The SiO2 mask layer was deposited by the PECVD method, and the photolithography process was done. Afterwards, the SiO2 layer was etched by the RIE method, satisfying the condition of 50 nm over etched within the etching rate of 140 nm/min.

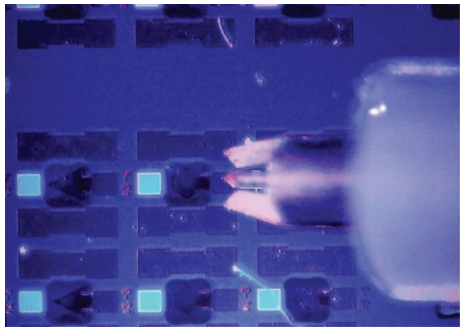

Figure 1: The FBAR array surface views under the microprobe of the probe station when the FBAR sensor was fixed on the probe station platform before experiment.

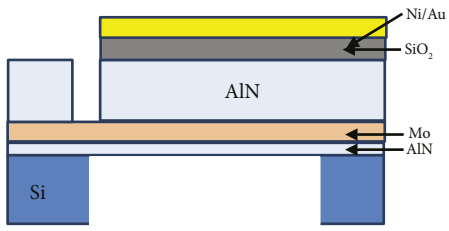

Figure 2: The design of AlN-based film bulk acoustic resonator. The piezoelectric material of the sensor is AlN.

The chip was consequently deep etched in the BOE solution (1 : 7) for 5 s. Ultimately the AlN layer etching was done with a stable etching rate of 177 nm/min. For the fourth step, the upper electrode deposition was done. The front side of the chip was processed with the photolithography step. After postbake and removing the photoresist, the step electron beam evaporation for the 30 nm/150 nm thickness Ti/Au was finished. Then, we conducted the stripping by the ultrasound metal stripping method. The last fabrication step of the whole FBAR process is back etching. Then, the photolithography process was done. After that, the SiO_2 layer was over etched for 50 nm. The crucial point of the back etch is deep silicon etching for 25 min with 150 cycles. The back side of the chip needs to be observed to check whether the deep silicon etching is correctly accomplished. After the deep silicon etching, the chip surface was cleaned to remove the surface oil. When the deep silicon etching step has been correctly finished, the chip would be cleaned by deionized water and baked in the oven. Thus, one group of FBAR chips could be fabricated successfully. The fabrication steps are listed in Figure 3. Above all the parameters of each photolithography are listed in Table 2.

3.2. Characterization. After device fabrication, the AlN-based FBAR sensor needs to be conducted characterization for checking the sensing material. In order to observe the piezoelectric material AlN surface after magnetron sputtering, the SEM and XRD characterization were done to scan the sensor surface. We conducted the SEM characterization for the AlN thin film of our FBAR, Figure 4 represent the SEM results. We could observe that there had been many particles on the silicon substrate, which was the AlN crystal

Table 1: The growth parameters comparison between AlN and Mo in sputtering process.

Parameters	AlN	Molybdenum
Nitrogen flow rate	100 sccm	
Argon flow rate	20 sccm	22 sccm
Target power	6 kW	6 kW
Target voltage	190 V	545 V
Forward power	209.8 W	0.1 W
Reflected power	0.9 W	0.1 W
Load power	209.4 W	0.1 W
Cavity background vacuum	$5e-8$ Torr	$5e-8$ Torr

of the thin film after sputtering. Table 1 was listed for the mechanical parameters of the AlN, Mo, and silicon substrate within our sensor design. Second, we conducted XRD characterization for the AlN thin film, which is shown in Figure 5 below. The XRD results revealed that there is a (002) AlN preferential orientation ($2\theta \approx 36^{\circ}$), besides the second peak is about $2\theta \approx 40^{\circ}$. The χ scan pattern shows that the c-axis of the AlN film is 18.5° inclined to the normal direction.

For the design of AlN-based FBAR sensor, we used several kinds of material, which are listed in Table 3 as below. The piezoelectric material AlN has stable physical properties and fine electrical characteristics. Besides, we conducted energy-dispersive X-ray spectroscopy (EDX) characterization and the EDX results have displayed the chemical element composition ratio of the AlN react area of the FBAR surface, which is shown in Figure 6 below. In Figure 6 the purple peak and the blue peak presents the Al chemical element and the *N* chemical element, respectively, which provides information about the AlN piezoelectric thin film.

4. Experiment and Sensor Signal

For sensor detection, we have measured the basic performance of our AlN-based FBAR sensor; the most important indexes of the FBAR include the resonance frequency and the quality factor (*Q*) [15]. After the index determination, we have found that the resonance frequency of our FBAR sensor is around 3.6 GHz and the quality factor (*Q*) is about 1050. The index quality factor (*Q*) represents the energy loss ratio of the resonant element; *Q* is a dimensionless unit [16]. The quality factor index figure of comparison between graphene and piezoelectric material AlN of this FBAR sensor is shown in Figure 7.

For the two target solutions, we collected the two samples from the laboratory within the common 100 ppm. During our measurement experiment, we secure our AlN-based FBAR chip on the surface of the probe station, and we drip the target solution onto electrode area of the FBAR sensor. Each time, we drip about 10 μL volume, and test for ethanol and acetone, respectively. The resonance frequency is recorded by the network analyzer. Before dropping the solution, we measure the initial resonance frequency with the FBAR sensor from the network analyzer, and after dropping the experimental solution, we measure the resonance frequency secondarily. Then, the two resonance frequency values are compared for both the ethanol sample and the acetone sample.

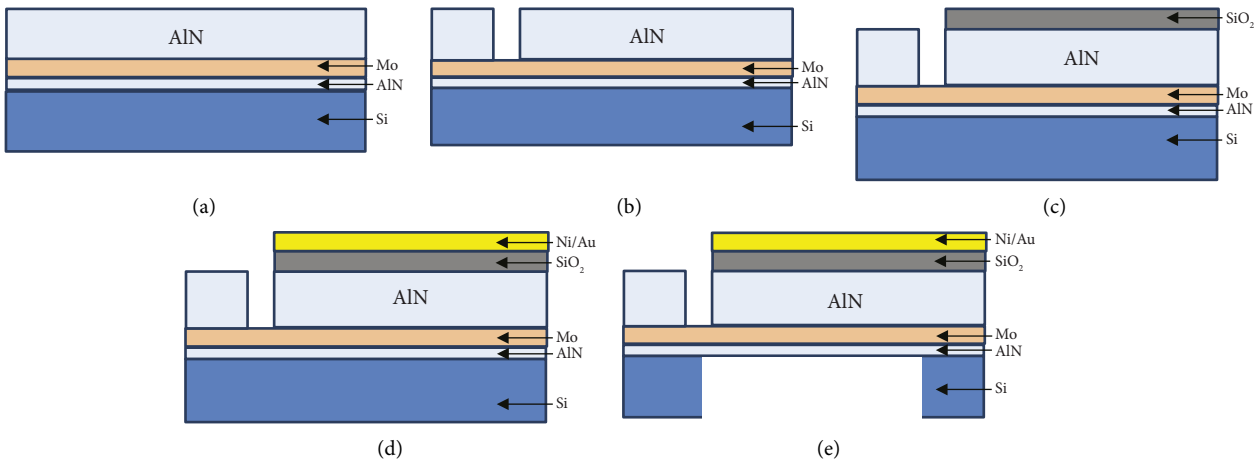

Figure 3: The illustration of fabrication protocol for FBAR chip. The upper electrode is Ni/Au, the bottom electrode is Mo. The piezoelectric material of the sensor is AlN. (b) Is for the photolithography and etching of the front side, (c) is for the SiO_2 deposition, (d) is for upper electrode deposition, (d) is for back etch.

Table 2: The photolithography parameters of the fabrication.

Which step	Photoresist	Exposure time
Second step	Front side: AZ 5214	Exposure 2 s—postbake 110°C 90 s—flood E 42 s
Third step	Front side: AZ 5214	Exposure 6.5 s, 45 s in developer
Fourth step	Front side: AZ 5214	Exposure 2 s—postbake 110°C 90 s—flood E 42 s
Fifth step	Both side: AZ4620	Exposure 22 s, 2 min in developer

During the measurement of acetone, we set the bias voltage ranging from −5 V to 5 V, with a 1 V increment for each one record. Before testing acetone, we measured the initial status of the FBAR sensor, then after adding acetone, the signal was recorded twice. For each one measurement, the peak frequency and the magnitude were recorded for the values. The two comparative figures below were the frequency and magnitude of the bias voltage +1 V. After acetone adding, the resonance frequency increased to 260 kHz when the bias voltage was kept at +1 V. For 100 ppm acetone, the resonance frequency increment would fluctuate as the bias voltage changed. For most bias voltage value, the resonance frequency increase about 250 kHz, except the circumstance for the +2 V, +3 V, and +4 V. Under these three values, the resonance frequency increment was below 200 kHz. Before acetone adding the magnitude was about −14.5 dB, while the magnitude changed to about −8 dB after dropping the acetone solution.

In our experiment, the comparative two figures of resonance frequency were done for the condition before acetone addition and after acetone addition, which are shown in Figures 8 and 9, respectively. The detailed resonance frequency values with its magnitude values are listed in Table 4.

In order to figure out the FBAR sensors' performance and sensitivity for different concentrations of the target analyst acetone, we prepared three acetone concentration samples and detected these three samples with the same module of our experiment FBAR sensor. For the experiment of different concentration measurements, we set the bias voltage near 0 V (about 0.1 V) to reduce the voltage's effects. After we measured the resonance frequency for the 0 ppm, 50 ppm, 100 ppm, and 150 ppm, we conducted the concentration measurement curve for acetone, which is shown in Figure 10. From the concentration curve, we could find the resonance frequency would increase with the concentration increment, while the curve would become saturated near the 150 ppm concentration; the sensor has significant sensitivity from 0 to 100 ppm range.

For sensing mechanism, after the acetone addition the adsorbed oxygen ions on the AlN thin film surface react with the acetone, and release CO_2 as a reaction product [17]. Thus, the surface chemical reaction would lead to the density change of the AlN film, resulting in the resonance frequency increase [18]. The reaction between acetone and the adsorbed oxygen is shown as follows [19]:

$$CH_3COCH_3 + O_2^- \longrightarrow CH_3^+ + CH_3O^- + CO_2 + e^-. \quad (1)$$

From the physical principle, it is demonstrated that the resonance frequency of the FBAR could be determined by the following equation [20]:

$$\Delta f = \frac{\sqrt{E}}{2\,d} \cdot \frac{(1 - \sqrt{1 - (\Delta\rho/\rho)})}{\sqrt{\rho - \Delta\rho}} = \frac{\sqrt{E}}{4\,d\rho\sqrt{\rho}} \cdot \Delta\rho, \quad (2)$$

where E, ρ and d are the elastic modulus, density and thickness of the AlN thin film, respectively. The variable v represents the acoustic velocity within the ZnO film and f is the resonance frequency of the FBAR [21]. From the (3) we could find that Δf is positively proportional to $\Delta\rho$, if the value of $\Delta\rho$ is positive value, the value Δf is influenced to be positive. It could illustrate the phenomenon that after adding acetone the resonance frequency of this FBAR sensor gets increased.

In room temperature, the oxygen is adsorbed at the AlN thin film surface of the FBAR, which is shown in the chemical balance equation as follows:

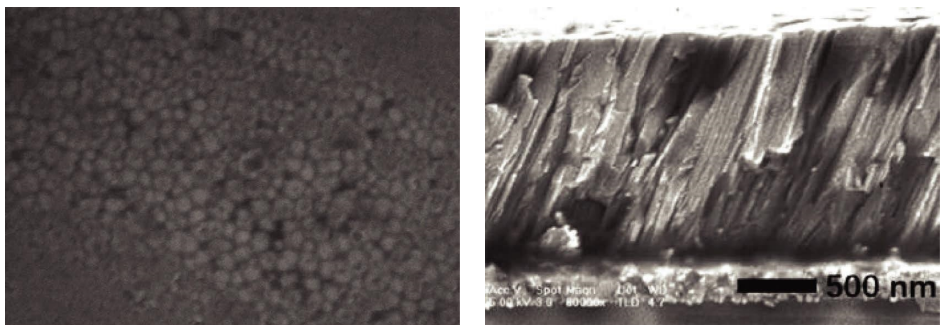

(a) (b)

Figure 4: The Scanning electron microscopy (SEM) pictures of the AlN thin film, (a) is for AlN surface morphology, (b) is for cross section view.

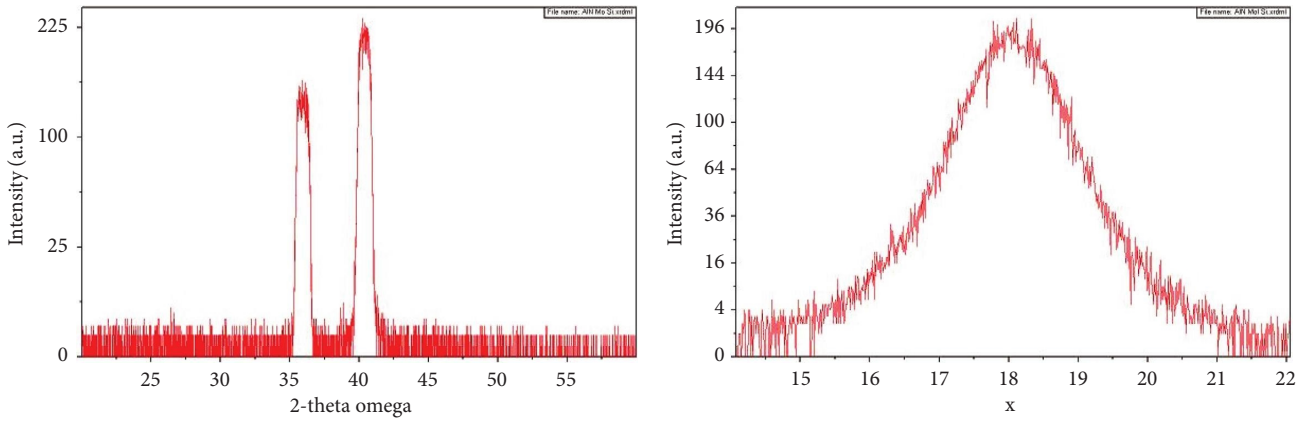

(a) (b)

Figure 5: X-ray diffraction (XRD) patterns of the AlN thin film, (a) 2θ scan; (b) χ scan of the AlN (002) peak.

$$CO_2 + H_2O + O_2 + e^- \underset{k_{-1}}{\overset{k1}{\rightleftharpoons}} k_1 O_2^{-1} + H_2CO_3. \quad (3)$$

In this equation e^- stands for a conduction electron at the surface, while k_1 and k_{-1} in this equation stands for the two rate constants, k_1 stands for the rate constant of forward reaction, k_{-1} stands for the rate constant of reverse reaction. When the oxygen gas upon the AlN surface becomes the dissolved oxygen within the AlN thin film, the target chemical acetone could be able to react with the dissolved oxygen [22]. The chemical reaction (1) would be influenced by the dissolved oxygen reaction [23], which is shown in equation (3).

From the relationship figure between gate voltage and resonance frequency in Figure 11, we could observe that the frequency shift keeps stable during the gate voltage sweep. During the whole detection experiment, the room temperature and room humidity were kept unchanged, and the experiment was conducted by the same person. From this point of view, we could deduce that the resonance frequency change is mainly due to the acetone addition, and other factors' influence is excludes.

During the measurement of ethanol, we set the bias voltage ranging from −5 V to 5 V, with a 1 V increment for each record. Before testing acetone, we measured the initial status of the FBAR sensor, and then, after adding ethanol the signal was recorded twice. The values of peak frequency and the magnitude were recorded at each measurement. The two comparative figures below were the frequency and magnitude of the bias voltage +1 V. We could observe that the peak frequency decreased after ethanol addition. With 100 ppm ethanol, the peak frequency decreased by about 1000 kHz compared to the situation before ethanol addition when the bias voltage was set at +1 V. For magnitude, the magnitude before ethanol addition was about −29.8 averagely, while after ethanol addition, the magnitude was about −9.3.

In our experiment, the comparative two figures of resonance frequency were done for the condition before ethanol addition and after ethanol addition, which are shown in Figures 12 and 13,respectively. The horizontal axis stands for the resonance frequency, and the vertical axis stands for the S_{11} parameter (unit: dB) in Figure 12 (before adding ethanol) and Figure 13 (after adding ethanol). The resonance frequency values and magnitude values were recorded during

Table 3: The physical material parameters of the FBAR sensor.

Parameter	Material		
	AlN	Molybdenum	Silicone
Density (kg/m^3)	3200	10000	2300
Young's modulus (GPa)	300	314.26	130
Poisson's ratio		0.31	0.28

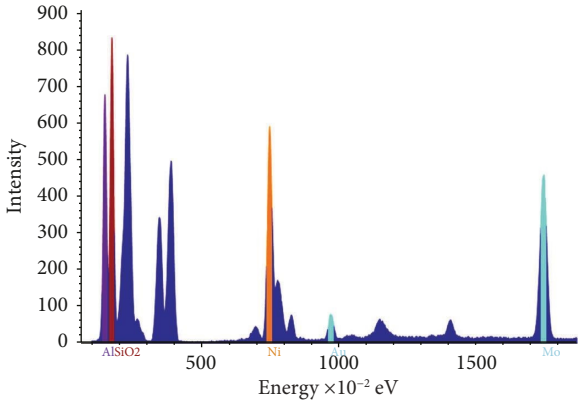

Figure 6: The energy-dispersive X-ray spectroscopy (EDX) characterization results for AlN area of FBAR sensor surface.

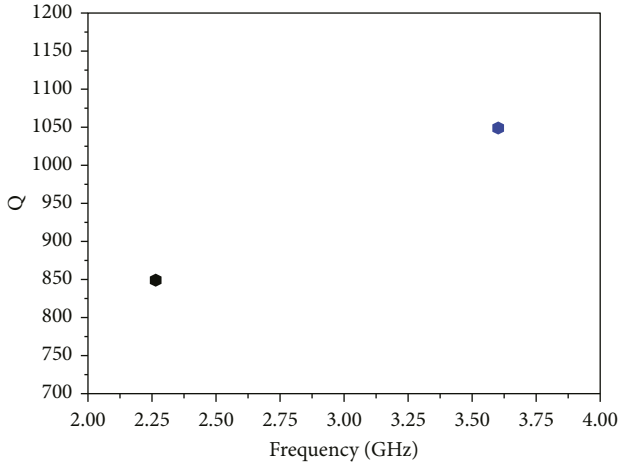

Figure 7: The quality factor (Q) figure comparison between graphene and AlN, black spot stands for graphene and blue spot stands for AlN in our sensor.

the measurement. The detailed resonance frequency values with its magnitude values are listed in Table 5.

For the sensing mechanism of ethanol detection, after ethanol addition, the adsorbed oxygen ions on the AlN thin film surface react with the acetone, releasing H_2O as the reaction product which is absorbed by the AlN thin film [24]. Under this circumstance the mass per unit area on the AlN surface has been influenced by the chemical reaction, causing the density to increase of this AlN thin film [25]. The density change of the AlN thin film would lead to the frequency decrease [26]. The reaction between ethanol and the adsorbed oxygen is shown as follows [27]:

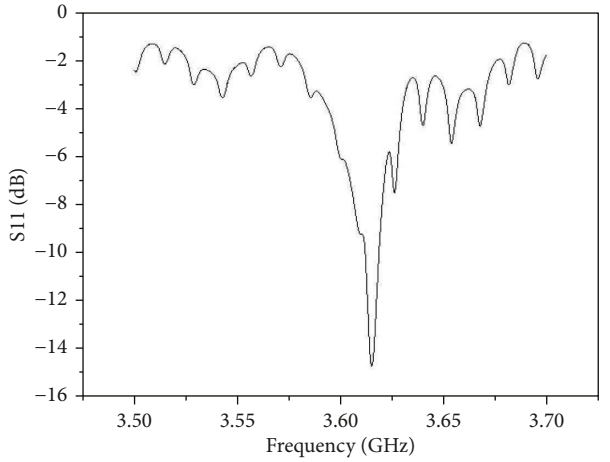

Figure 8: The resonance frequency figure of the AlN-based FBAR sensor before adding acetone, the horizontal axis is frequency while the vertical axis is S_{11} parameter.

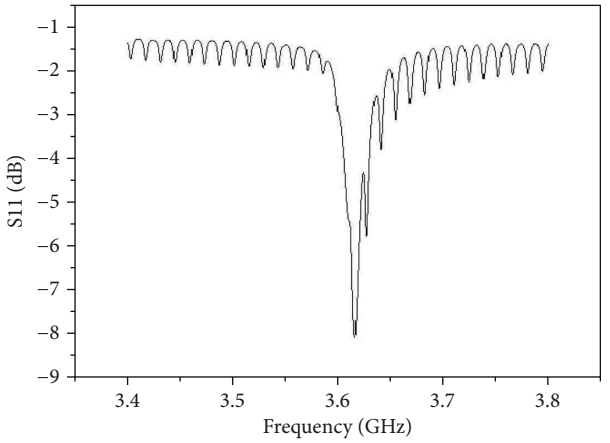

Figure 9: The resonance frequency figure of the AlN-based FBAR sensor after adding acetone, the horizontal axis is frequency while the vertical axis is S_{11} parameter.

$$C_2H_5OH + O_2^- \longrightarrow CH_3COOH + H_2O + e^-. \quad (4)$$

From the (4) we could deduce that Δf is negatively proportional to $\Delta\rho$ [28], if the value of $\Delta\rho$ is positive value, the value Δf is influenced to be minus [29]. The (4) could explain the negative correlation relationship between the resonance frequency change and the ethanol addition [30].

From the relationship figure between gate voltage and resonance frequency in Figure 14, we could observe that except for the gate voltage of +2 V, the frequency shift keeps stable. During the whole detection experiment, the room temperature and room humidity were kept unchanged, and the experiment was conducted by the same person. From this point of view, we could deduce that the resonance frequency change is mainly due to the ethanol addition, and other factors' influence is excludes. Besides, we conducted the ethanol concentration measurement experiment and finished the ethanol

Table 4: The resonance frequency comparison of before and after adding acetone solutions.

Voltage	Initial state (GHz)	Magnitude	After adding acetone (GHz)	Magnitude
+5 V	3.61532	−14.29567	3.61559	−8.0435
+4 V	3.61536	−14.3501	3.61553	−8.04806
+3 V	3.61528	−14.40813	3.61547	−8.05437
+2 V	3.61532	−14.50763	3.61545	−8.05346
+1 V	3.61517	−14.7065	3.61543	−8.05768
0	3.6151	−15.85078	3.61541	−8.06339
−1 V	3.61518	−14.46039	3.61543	−8.06564
−2 V	3.61509	−14.53756	3.61533	−8.07524
−3 V	3.61505	−14.5795	3.61531	−8.08173
−4 V	3.61499	−14.64694	3.61527	−8.08585
−5 V	3.6149	−14.70183	3.61525	−8.08964

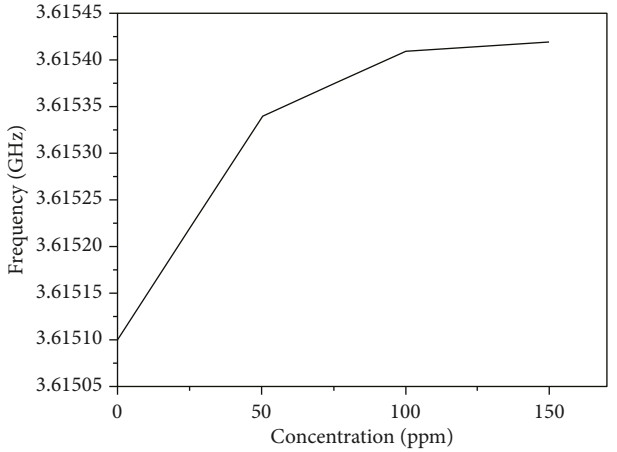

Figure 10: The concentration measurement results for the acetone samples.

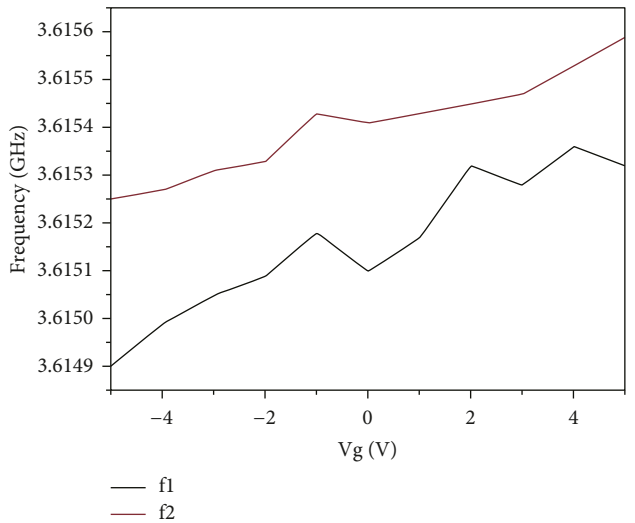

Figure 11: The figure for influence of gate voltage change on the resonance frequency shift value during acetone experiment. The black curve f_1 stands for the resonance frequency before acetone addition, the red curve f_2 stands for the resonance frequency after acetone addition.

concentration figure. We prepared three ethanol concentration samples and detected these three samples with the same module of our experiment FBAR sensor. For the

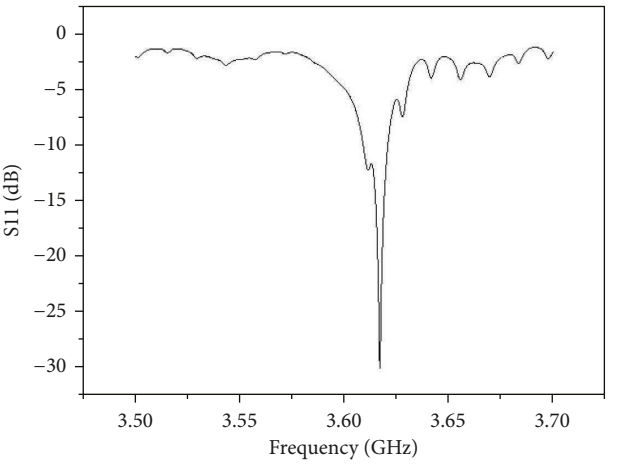

Figure 12: The resonance frequency figure of the AlN-based FBAR sensor before adding ethanol, the horizontal axis is frequency while the vertical axis is S_{11} parameter.

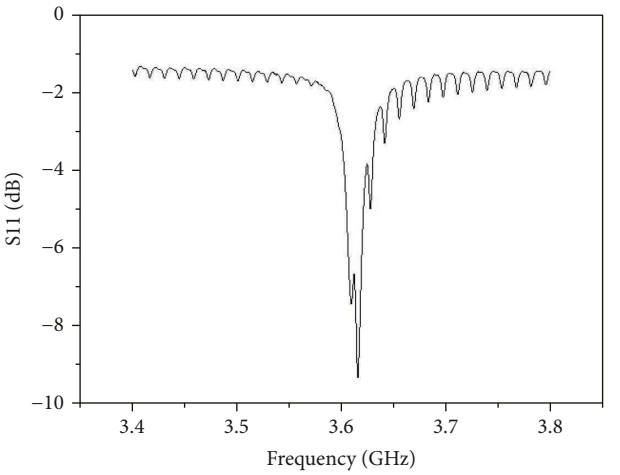

Figure 13: The resonance frequency figure of the AlN-based FBAR sensor after adding ethanol, the horizontal axis is frequency while the vertical axis is S_{11} parameter.

experiment of different concentration measurements, we set the bias voltage near 0 V (about 0.1 V) to reduce the voltage's effects. After we measured the resonance frequency for the 0 ppm, 50 ppm, 100 ppm, and 150 ppm, the concentration figure of ethanol is finished in

Table 5: The resonance frequency comparison of before and after adding ethanol solutions.

Voltage	Initial state (GHz)	Magnitude	After adding acetone (GHz)	Magnitude
+5 V	3.617	−29.4286	3.61593	−9.36744
+4 V	3.61691	−29.63381	3.61593	−9.35297
+3 V	3.61688	−29.49053	3.61587	−9.33251
+2 V	3.61681	−29.85427	3.61583	−9.32041
+1 V	3.61674	−30.07379	3.61579	−9.30655
0	3.61672	−29.7705	3.61571	−9.27577
−1 V	3.6167	−29.83415	3.61585	−9.31602
−2 V	3.61663	−29.83533	3.61575	−9.30397
−3 V	3.61658	−29.75886	3.61571	−9.28899
−4 V	3.61654	−29.84557	3.61568	−9.31822
−5 V	3.61646	−29.99142	3.61568	−9.29297

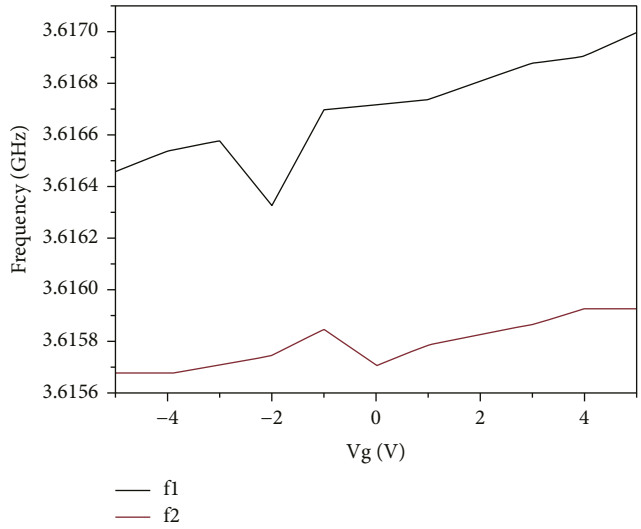

Figure 14: The figure for influence of gate voltage change on the resonance frequency shift value during ethanol experiment. The black curve f_1 stands for the resonance frequency before ethanol addition, the red curve f_2 stands for the resonance frequency after ethanol addition.

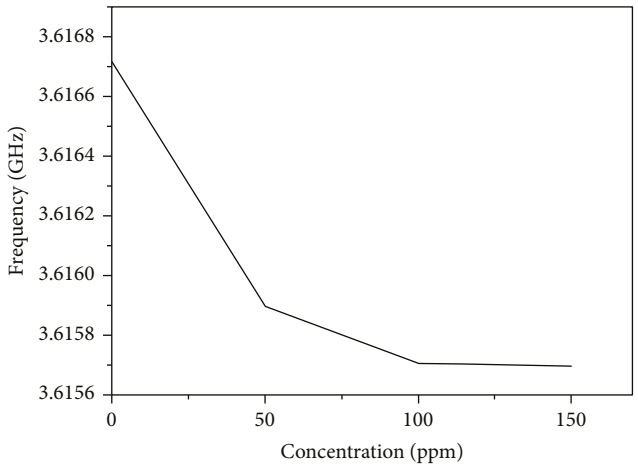

Figure 15: The concentration measurement results for the ethanol samples.

Figure 15. From the concentration curve, we could find the sensor has significant sensitivity from 0 to 100 ppm. The real-time frequency shift figures are shown in Figure 16 below. For acetone and ethanol, the real-time curve was recorded under a 0 V voltage.

After the detection experiment, we have summarized some sensor reliability data of our FBAR sensor. The AlN-based FBAR could distinguish acetone and ethanol from 0 ppm to near 150 ppm in laboratory measurement. Among one fabrication batch of FBAR devices, about 95% of the devices could be able to detect sensor signals. For one FBAR chip, about 92% of the modules could effectively detect the analyst. The FBAR working temperature is from −30°C to 50°C, for general use and high precision testing the FBAR works under room temperature because extreme temperatures would lead to temperature drift for frequency measurement. The temperature coefficient of the FBAR sensor is usually 20 to −35 ppm/°C. But recently, the Suzhou Institute of Nano-tech and Nano-Bionics had conducted the research of temperature fluctuation compensation system within the FBAR sensor; thus, the temperature drift's influence on frequency measurement would be weakened to some extent [31]. Above all, we calculated the sensitivity of this AlN FBAR sensor for acetone and ethanol detection, and compared it with the ZnO FBAR in previous literature [32]. The sensitivity indexes are listed in Table 6. The mean time to failure of our FBAR chips is about 28.5 days based on our failure analysis.

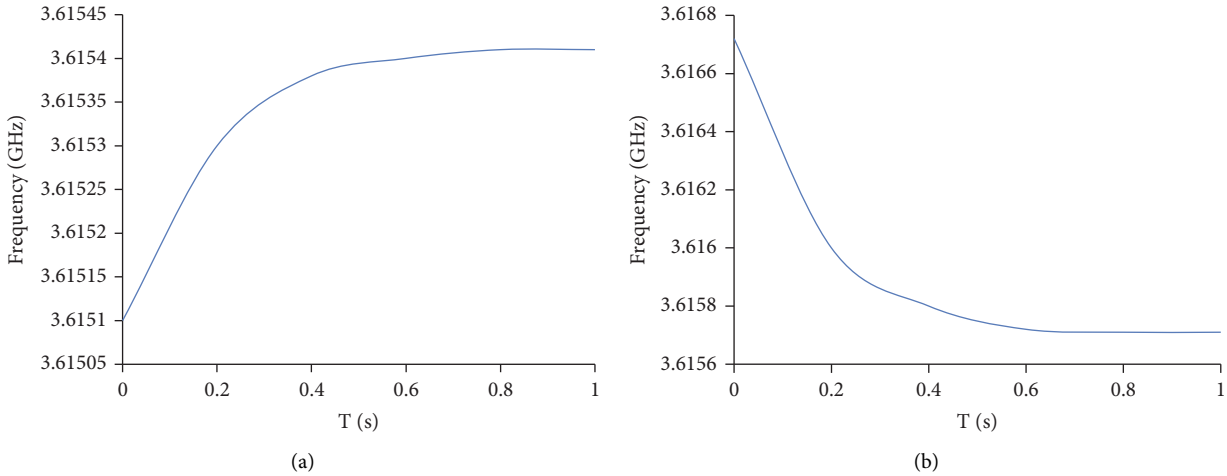

Figure 16: The real-time frequency shift curves for acetone and ethanol detection. (a) The real-time frequency shift for acetone detection. (b) The real-time frequency shift for ethanol detection.

Table 6: The AlN FBAR sensitivity compared with ZnO FBAR.

	Acetone (kHz/ppm)	Ethanol (kHz/ppm)
AlN FBAR	1.6	3.9
ZnO FBAR	1.3	1.6

5. Conclusions

In summary, we have developed an AlN-based FBAR sensor and conducted acetone and ethanol sensing experiment using this FBAR sensor. From our experiment, we could find that the resonance frequency of our FBAR sensor increases after the acetone sample addition, while the FBAR sensor presents the opposite response after ethanol addition. For acetone detection's sensing mechanism, the acetone reacts with the free oxygen within the AlN surface, the reaction products include CO_2 and other ions which would volatilize or dissolve. The AlN thin film's entire thickness tends to be attenuated by this chemical reaction, and the film density tends to be increased. In this case, this property change is in charge of the frequency upshift. On the other side, for ethanol detection's sensing mechanism, the ethanol reacts with the oxygen ions within the AlN surface; the reaction products include H_2O and acetic acid. The AlN thin film's entire thickness tends to grow thicker due to this chemical reaction, because the reaction products are nonvolatile liquid. In that case the density of the AlN thin film tends to decrease, so the peak resonance frequency is attenuated. Furthermore, this AlN-based FBAR sensor could be used to detect other kinds of chemical volatile gases. However, our this work only conducted the FBAR sensor for detection of those two VOCs commonly used in laboratory, for more complex volatile organic compounds, the FBAR surface needs to be modified by the special chemical functional groups. In that case, with the concern of selectivity, more experiments would be scheduled to study the sensing mechanism of FBAR to different targets by different functionalization processes. The research significance of FBAR sensor needs to be deeply demonstrated and understood from laboratory experiments and sensor theoretical study, ultimately realizing microminiaturization and diversity detection.

Data Availability

The data are collected from Our own experiment.

Conflicts of Interest

The authors declare that they have no conflicts of interest.

Acknowledgments

This paper's project was supported by the research start-up funding No. GY-Z20045 of Fujian University of Technology. The authors are grateful to Professor Bao-Shun Zhang for his project supports, and Wen-Kui Lin for his experimental assistance from Suzhou Institute of Nano-tech and Nano-Bionics, Chinese Academy of Science. The authors also sincerely appreciate Professor Guan-Wen Zhang and Professor Jiang-Han Chen's help from Guangdong Institute of Analysis (China National Analytical Guangzhou), the experiment was conducted with their technical guidance and suggestions.

References

[1] A. Tuneli, H. Bag, and A. R. Turker, "Spectrophotometric determination of some pesticides in water samples after preconcentration with *Saccharomyces cerevisiae* immobilized on sepiolite," *Fresenius' Journal of Analytical Chemistry*, vol. 371, pp. 1134–1138, 2001.

[2] L. Qin, Q. Chen, H. Cheng, Q. Chen, J. F. Li, and Q. M. Wang, "Viscosity sensor using ZnO and AlN thin film bulk acoustic resonators with tilted polarc-axis orientations," *Journal of Applied Physics*, vol. 110, no. 9, Article ID 094511, 2011.

[3] L. F. Capitan-Vallvey, M. K. A. Deheidel, and R. Avidad, "Determination of carbaryl in foods by solid-phase room-temperature phosphorimetry," *Fresenius' Journal of Analytical Chemistry*, vol. 362, pp. 307–312, 1998.

[4] D. Chen, J. J. Wang, D. H. Li, and Y. Xu, "Hydrogen sensor based on Pd-functionalized film bulk acoustic resonator," *Sensors and Actuators B: Chemical*, vol. 159, pp. 234–237, 2011, 1.

[5] R. C. Lin, Y. C. Chen, W. T. Chen, C. C. Cheng, and K. S. Kao, "Highly sensitive mass sensor using film bulk acoustic resonator," *Sensors and Actuators: Sensors and Actuators A: Physical*, vol. 147, no. 2, pp. 425–429, 2008.

[6] W. Pang, H. Zhao, E. S. Kim, H. Zhang, H. Yu, and X. Hu, "Piezoelectric microelectromechanical resonant sensors for chemical and biological detection," *Lab on a Chip*, vol. 12, pp. 29–44, 2012, 1.

[7] G. Sharma, L. Liljeholm, J. Enlund, J. Bjurstrom, I. Katardjiev, and K. Hjort, "Fabrication and characterization of a shear mode AlN solidly mounted resonator-silicone microfluidic system for in-liquid sensor applications," *Sensors and Actuators A: Physical*, vol. 159, pp. 111–116, 2010, 1.

[8] G. Wingqvist, "AlN-Based sputter-deposited shear mode thin film bulk acoustic resonator(FBAR) for biosensor applications," *Surface and Coatings Technology*, vol. 205, pp. 1279–1286, 2010, 5.

[9] M. Zhang, L. Du, F. Zhen, and Z. Zhao, "A sensitivity-enhanced film bulk acoustic resonator gas sensor with an oscillator circuit and its detection application," *Micromachines*, vol. 8, pp. 1–11, 2015, 1.

[10] A. Kumar and R. Prajesh, "The potential of acoustic wave devices for gas sensing applications," *Sensors and Actuators A: Physical*, vol. 339, no. 1, p. 113498, 2022.

[11] A. Soltan, R. Sadeghzadeh, and S. Mohammad-Ali-Nezhad, "Microwave sensor for liquid classification and permittivity estimation of dielectric materials," *Sensors and Actuators A: Physical*, vol. 336, p. 113397, 2022.

[12] A. Lin, H. Yu, and M. S. Walters, "Explosive trace detection with FBAR-based sensor," *IEEE International Conference on Micro Electro Mechanical Systems*, vol. 365, p. 10978, 2015.

[13] Z. Zhao, Z. Qian, and Y. K. Yong, "Frequency shift prediction of a shear mode multi-layered FBAR sensor in viscous media using transfer matrix method," *Applied Mathematical Modelling*, vol. 99, pp. 555–565, 2021.

[14] J. Wang, D. Chen, Y. Xu, and W. Liu, "Label-free immunosensor based on micro-machined bulk acoustic resonator for the detection of trace pesticide residues," *Sensors and Actuators B: Chemical*, vol. 190, pp. 378–383, 2014.

[15] Y. Kumar, K. Rangra, and R. Agarwal, "Design and simulation of FBAR for quality factor enhancement," *Mapan*, vol. 32, no. 2, pp. 113–119, 2017.

[16] S. Parolai, "Shear wave quality factor *Qs* profiling using seismic noise data from microarrays," *Journal of Seismology*, vol. 18, no. 3, pp. 695–704, 2014, 1.

[17] X. Qiu, R. Tang, J. Zhu et al., "Acetone sensor based on film bulk acoustic resonator," *IEEE Sensors 2010 conference*, vol. 299, p. 178, 2010.

[18] D. Chen, J. Wang, Y. Wu, and D. Li, "A pure shear mode ZnO film resonator for the detection of organophosphorus pesticides," *Sensors and Actuators B: Chemical*, vol. 171, pp. 1081–1086, 2012, 1.

[19] S. Song, D. Chen, H. Wang et al., "Shear mode bulk acoustic resonator based on inclined c-Axis AlN film for monitoring of human hemostatic parameters," *Micromachines*, vol. 9, no. 10, p. 501, 2018.

[20] M. Zhang, L. Du, Z. Fang, and Z. Zhao, "Micro through-hole array in top electrode of film bulk acoustic resonator for sensitivity improving as humidity sensor," *Procedia Engineering*, vol. 120, pp. 663–666, 2015.

[21] J. Liu, Y. Yuan, Z. Ren, Q. Tan, and J. Xiong, "High-temperature dielectric properties of aluminum nitride ceramic for wireless passive sensing applications," *Sensors*, vol. 15, no. 9, pp. 22660–22671, 2015.

[22] J. Liu, Z. Zhao, Z. Fang, Z. Liu, Y. Zhu, and L. Du, "High-performance FBAR humidity sensor based on the PI film as the multifunctional layer," *Sensors and Actuators B: Chemical*, vol. 308, p. 127694, 2020.

[23] T. Mirea, J. Olivares, M. Clement, and E. Iborra, "Impact of FBAR design on its sensitivity as in-liquid gravimetric sensor," *Sensors and Actuators A: Physical*, vol. 289, pp. 87–93, 2019, 15.

[24] X. Qiu, J. Oiler, J. Zhu et al., "Film bulk acoustic-wave resonator based relative humidity sensor using ZnO films," *Electrochemical and Solid-State Letters*, vol. 13, pp. J65–J67, 2010, 5.

[25] L. Wang, A. Lin, and E. S. Kim, "Miniature sensing system with FBAR-based oscillators and frequency shift detector," *IEEE Sensors Journal*, vol. 18, pp. 7633–7637, 2018, 18.

[26] M. Zhang, L. Du, Z. Fang, and Z. Zhao, "Micro through-hole array in top electrode of film bulk acoustic resonator for sensitivity improving as humidity sensor," *Procedia Engineering*, vol. 120, pp. 663–666, 2015.

[27] H. Guo, Y. Gao, and T. Liu, "A theoretical study of the VOC sensor based on polymer-coated diaphragm embedded with FBAR," *Measurement*, vol. 129, pp. 206–210, 2018.

[28] H. Guo, A. Guo, Y. Gao, and T. Liu, "Influence of external swelling stress on the frequency characteristics of a volatile organic compound (VOC) sensor based on a polymer-coated film bulk acoustic resonator (FBAR)," *Instrumentation Science & Technology*, vol. 48, pp. 431–442, 2020, 4.

[29] J. Koo, K. Wang, and R. Rudy, "A 2GHz FBAR based transformer coupled oscillator design with phase noise reduction," *Circuits and System II: Express Briefs IEEE Transactions on(IEEE T Circuits-II)*, vol. 99, pp. 1–5, 2018, 1.

[30] T. Jamneala, P. Bradley, A. Shirakawa, R. K. Thalhammer, and R. Ruby, "An investigation of lateral modes in FBAR resonators," *IEEE Transactions on Ultrasonics, Ferroelectrics, and Frequency Control*, vol. 63, pp. 778–789, 2016, 5.

[31] W. Lin, X. Yun, Z. Zeng et al., "Super-high sensitivity FBAR temperature sensor based on size effect of Ti insertion layer," *Materials Research Express*, vol. 8, p. 095701, 2021.

[32] Y. Jiang, Y. Chang, C. Gao, B. Liu, and X. Duan, "Flexible volatile organic compounds sensor based on thin-film bulk acoustic resonator," *Chinese Journal of Sensors and Actuators*, vol. 31, pp. 1461–1466, 2018, 10.